CONF-9605203--1
ANL/XFD/CP--90210

Off-Specular X-Ray Scattering Studies of the Morphology of Thin Films

S.K. Sinha,[a] Y. P. Feng,[a] C.A. Melendres,[b] D.D. Lee,[c] T.P. Russell,[d] S.K. Satija,[e] E.B. Sirota,[f] M.K. Sanyal[g]

[a]*Experimental Facilities Division, Advanced Photon Source, Argonne National Laboratory, Argonne, IL 60439, USA*

[b]*Chemical Technology Division, Argonne National Laboratory, Argonne, IL 60439*

[c]*Nuclear Engineering Department, Massachuccetts Institute of Technology, Cambridge, MA 02139*

[d]*IBM Almaden Research Center, San Jose, CA 95120*

[e]*National Institute for Standards and Technology, Gaithersburg, MD 20899, USA*

[f]*Corporate Research, Exxon Research and Engineering Company Annandale, NJ 08801*

[g]*Saha Institute of Nuclear Physics, Calcutta, India*

We discuss the scattering of x-rays from thin films at a surface or interface decorated with a morphology of islands and how these effects manifest themselves in the specular reflectivity and the diffuse (off-specular) scattering. We show how this technique has been used to study block copolymer films decorated with islands on the surface and the development of electrochemically induced pitting on a Cu electrode in an electrolyte solution.

The availability of synchrotron radiation has made it possible to study in detail the *in situ* structure and morphology of films absorbed on solid or liquid surfaces. Specular x-ray reflectivity studies have been used to study the laterally averaged density profile of the films along the surface-normal direction, and off-specular scattering and grazing incidence diffraction have been used to study the in-plane structure. Scattering methods are in a sense complementary to various types of surface imaging microscopies, such as AFM, STM, etc., but have the advantage of being able to provide **global** statistical information about the surface without the need for digitizing and averaging the images. They also have the capability to probe buried interfaces with very high resolution. In this paper, we shall review synchrotron scattering studies of the surface morphology and wetting properties of polymer films on solid substrates and of the morphology of pitted films obtained by the process of electrochemical corrosion.

Consider a surface or interface consisting of a series of islands or pits on a flat reference interface as shown in Fig. 1. The scattering process is indicated schematically. $\bar{k}_0$ is the incident wavevector for the x-rays at grazing angle of incidence α, $\bar{k}_1$ is the scattered x-ray wavevector at grazing angle of scattering β, and the wavevector transfer $\bar{q} = \bar{k}_1 - \bar{k}_0$. We assume for simplicity that there is no correlation between the height of the islands and their lateral dimensions or spacing. Assuming that the material inside the islands and the

substrate is uniform, the Born approximation for the scattering from such an interface yields the scattering function [1]

$$S(\bar{q}) = \frac{(\Delta\rho)^2}{q_z^2} \int\int\int\int dx dy dx' dy' \; e^{-iq_z[z(x,y)-z(x',y')]} \; e^{-i[q_x(x-x')+q_y(y-y')]} \qquad (1)$$

where z is the direction normal to the average interface, $(\Delta\rho)$ is the electron density contrast across the interface, and z(x, y) is the interface profile as a function of lateral position. If h(z) is the height distribution function of the islands, we may define its Fourier transform

$$h(q_z) = \int_{-\infty}^{\infty} dz \; h(z) \, e^{-iq_z z} \qquad (2)$$

If $h(z)$ is positive for positive z, we have islands, while if $h(z)$ is positive for negative z, we describe pits. We may also define the average form factor of each island

$$f(q_1) = \left\langle \frac{1}{A_0} \int d\bar{r} \; e^{-i\bar{q}_1 \bar{r}} \right\rangle \qquad (3)$$

where the integration is over the surface area (A_0) of the island, and $\bar{q}_1$ is the in-plane component of $\bar{q}$. If ϕ is the fractional coverage of the surface by the islands, then it may be shown that [2]

$$S(\bar{q}) = S_{spec}(\bar{q}) + S_{diff}(\bar{q}) \qquad (4)$$

where

$$S_{spec} = \frac{(\Delta\rho)^2}{q_z^2} 4\pi^2 A \delta(q_x)\delta(q_y)\left|(1-\phi) + \phi h(q_z)\right|^2 \qquad (5)$$

The total surface area is A and represents the specular reflectivity, while the off-specular scattering is given by

$$S_{diff}(\bar{q}) = \frac{(\Delta\rho)^2}{q_z^2} \phi A A_0 \left|f(\bar{q}_1)\right|^2 \left[S(\bar{q}_1)\left|1 - h(q_z)\right|^2 + \left\{1 - \left|h(q_z)\right|^2\right\}\right] \qquad (6)$$

where $S(\bar{q}_1)$ represents the in-plane structure factor of the islands,

$$S(\bar{q}_1) = \frac{1}{N}\left\langle \sum_{lm} e^{-i\bar{q}_1(\bar{r}_l - \bar{r}_m)} \right\rangle - 4\pi^2(\phi/A_0)\delta(q_x)\delta(q_y) \qquad (7)$$

$\bar{r}_l$, $\bar{r}_m$ represent the island center positions, and N is the total number of islands. (A is the total surface area.) The second term subtracts the contribution of the average island density, which contributes only to $S_{spec}(\bar{q})$. Thus the specular reflectivity yields information on the island height distribution function, while the off-specular yields the in-plane correlations between the islands. If there are strong nearest neighbor correlations, $S(\bar{q})$ will have side peaks at finite $\bar{q}_1$, provided the distance between neighbors is within the x-ray coherence length across the surface (typically 10 μ-20 μ for a synchrotron experiment). In this sense, off-specular scattering is the analogue, for the in-plane structure, of small-angle scattering for bulk colloidal liquids (c.f. the work of S.H. Chen and collaborators), but with far smaller $\bar{q}$-vectors (and consequently much larger length scales) accessible. An expression that is more accurate than the Born approximation is that given by the so-called Distorted Wave Born Approximation (DWBA) [1] in which the scattered intensity is given by

$$I(\bar{q}) = |T(\alpha)|^2 |T(\beta)|^2 S(\tilde{q}) \qquad (8)$$

Here $T(\alpha)$ is the Fresnel transmission coefficient for the average surface at grazing angle of incidence α, and $S(\tilde{q})$ is the Born approximation expression with $\bar{q}$ replaced by its value **inside** the medium under the interface, i.e., modified by the refractive index of the medium. (Except near the critical angle for total reflection, this difference is usually negligible.)

Previous neutron reflectivity measurements [3] have shown that annealed thin films of diblock copolymers of polystyrene (PS) and polymethylmethacrylate (PMMA) form a highly oriented lamellar morphology parallel to the substrate surface. In the neutron reflectivity measurements, a high degree of scattering contrast between the PS and PMMA layers was achieved by deuterating one of the blocks while leaving the other hydrogenated. The reflectivity profile showed the typical small-angle Bragg peaks associated with the lamellar ordering, and fitting this profile yielded details of the interfacial structure between the PS and PMMA blocks. The top **surface** of the annealed PS-PMMA diblock copolymer films shows an unusual morphology consisting of islands of varying size. [4, 5] These islands are of constant thickness above the surface and presumably correspond to a bilayer that cannot completely cover the surface. For x-rays, the contrast between the PS and PMMA blocks is negligible, so to a good approximation we may consider the problem as that of scattering from a uniform film with islands of constant thickness on the surface. If the thickness of the islands is Δ, then

$$h(q_z) = e^{-iq_z\Delta}, \qquad (9)$$

and Eq. (6) may be written as

$$S_{diff}(\vec{q}) = 4\frac{(\Delta\rho)^2}{q_z^2}\phi A A_0 \left|f(q_1)\right|^2 S(q_1)\mathrm{Sin}^2\left(\frac{q_z\Delta}{2}\right), \qquad (10)$$

while from Eq. (5), the specular reflectivity may be written as

$$R(q_z) = R_F(q_z)\left[1-4\phi(1-\phi)\mathrm{Sin}^2\left(\frac{q_z\Delta}{2}\right)\right], \qquad (11)$$

where $R_F(q_z)$ is the Fresnel reflectivity $\left(=16\pi^2(\Delta\rho)^2/q_z^4\right)$ in the Born approximation. For $q_1 \cong 0$ (i.e., close to specular), $|f(q_1)| \cong 1$ and $S(q_1) \rightarrow$ constant, and Eqs. (10) and (11) show that the diffuse scattering and the specular reflectivity both show modulations of period $(2\pi/\Delta)$ along q_z, due to the islands but exactly **out of phase** with each other. If the polymer film is on a smooth substrate and itself has thickness t (apart from the islands), the diffuse scattering will be unchanged, but the specular reflectivity will be modified by the substrate to yield

$$R(q_z) = \frac{16\pi^2}{q_z^4}\left\{\rho_1^2 e^{-q_z^2\sigma_1^2}\left[1-4\phi(1-\phi)\mathrm{Sin}^2\left(\frac{q_z\Delta}{2}\right)\right] + (\rho_2-\rho_1)^2 e^{-q_z^2\sigma_2^2}\right.$$
$$\left. + 2\rho_1(\rho_2-\rho_1)e^{-\frac{1}{2}q_z^2(\sigma_1^2+\sigma_2^2)}\left[\phi\mathrm{Cos}(q_z(t+\Delta)) + (1-\phi)\mathrm{Cos}(q_z t)\right]\right\}, \qquad (12)$$

where ρ_1 is the electron density of the film and ρ_2 that of the substrate. In Eq. (12), we have allowed for additional roughness at the film/air interface (σ_1) and at the substrate/film interface (σ_2). In addition to the modulations of period $(2\pi/\Delta)$, the specular reflectivity will contain rapid modulations of period $(2\pi/t)$ (the so-called "Kiessig Fringes") due to the overall film thickness. These Kiessig fringes will also be present in the diffuse scattering as a function of q_z if there is a degree of **conformal** roughness between the two film interfaces (as is usually the case), [6,7] but in this case these modulations will be **in phase** in both the diffuse and the specular scattering.

These phenomena are illustrated in x-ray specular and diffuse scattering experiments carried out on the PS/PMMA (50:50) samples discussed above at the Exxon beamline (X10A) at the NSLS, Brookhaven. Fig. 2 illustrates the specular reflectivity and longitudinal diffuse scattering ($q_z \cong 0$) as a function of q_z for the PS/PMMA film of MW 30,000 on a silicon substrate.

From the earlier neutron reflectivity measurements, [3] it was shown that the PS block preferentially locates at the air/film interface and the PMMA at the film/substrate interface, with the layer thickness at these interfaces equal to one-half of the bilayer thickness. Given this constraint, the multilayer film can have only (n + 1/2) number of bilayers (where n is an integer). The

specular reflectivity analysis of the Kiessig fringes yielded in the present case 9.5 bilayers in a total film thickness of 1496 Å, or 176 Å/bilayer, in good agreement with the neutron measurements. Fig. 2 shows additional modulations in both the specular and diffuse scattering due to islands of thickness 176 Å on the top surface of the film, and these modulations are out of phase, as predicted. The diffuse scattering also shows the total-film-thickness-induced Kiessig fringes due to conformal roughness between the film/air and film/substrate interfaces. Diffuse scattering as a function of q_t (transverse diffuse scans) revealed the islands to have a lateral size of ~ 5 μ. A quantitative fit to the specular and diffuse scattering was obtained after making certain assumptions about the roughness parameters. For another sample of PS/PMMA (50:50) of MW 100,000, the modulations due to the islands could not be seen in the diffuse scattering, because the island sizes had grown laterally to 25 μ, i.e., greater than the x-ray coherence length across the surface. The above experiments were done for symmetric diblock copolymers. Experiments have also been carried out on asymmetric triblock polyvinylpyridine (PVP) - polystyrene (PS) - PVP copolymer films, where the volume fraction of PVP was 0.25, using transmission electron microscopy, atomic force microscopy, secondary ion mass spectrometry and neutron and x-ray reflectivity. [8] Very similar experiments and analyses of polymer films have also been done independently by Cai et al. [9]

We now discuss some recent experiments which apply similar methods to study the details of pitting corrosion on a metal surface in an electrochemical cell. By measuring x-ray diffuse scattering from electron density voids created by the pits as a function of time at the pitting potential, we were able to probe, at the early stages of pitting, the micromorphology and evolution of the pits. A preliminary account of these experiments was recently published. [10]

We employed an x-ray/electrochemical cell in the transmission geometry, which was used in the previous work, [11, 12] to reduce the amount of x-ray absorption by the electrolyte and to allow small scattering angles. The electrode was made of a thin Cu film (~1500 Å in thickness) deposited on a polished silicon substrate and had an active electrode area of 3.2 mm x 10 mm. The cell was fitted with two 25 *m*m thick Teflon (FEP) widows separated by 3.2 mm to hold the electrolyte and to allow x-ray access to the electrode surface. The electrolyte was a 0.01 M $NaHCO_3$ solution, which is known to induce pitting corrosion on Cu surfaces in the absence of Cl^- ions. [13] The solution was prepared using high purity water (resistivity ~ 18 MWcm) and reagent grade chemicals. The electrochemical instrumentation consisted of a Princeton Applied Research Model 173 potentiometer, a Model 175 universal programmer and a Hewlett Packard Model 7045 XY plotter.

Both x-ray specular and off-specular reflectivity were measured at a few fixed applied potentials to study the general and localized corrosion. Specular reflectivity of the Cu electrode was first measured and used to characterize its surface roughness in the absence of pits. Fig. 3 shows reflectivities taken at applied potentials of - 0.9 V where the Cu surface was free of oxide film and of + 0.2 V where the Cu surface is passivated. Assuming that the morphology of the electrode surface at both potentials was statistically Gaussian, a rms roughness of 18 Å for -0.9 V and 22 Å for + 0.2 V was obtained by fitting the

measured reflectivity with the DWBA method. [1] The reduction in the rms roughness in the cathodic region is consistent with experimental findings of You *et. al.* [11] Off-specular reflectivity (rocking curve) was also measured at these two potentials and fitted to a model of surface scaling, [1] which indicated that the lateral correlation length of the surface roughness was less than 100 Å.

To study the development and evolution of pits as a function of pitting time, the applied potential was scanned at a rate of 10 mV/sec from the open circuit potential (~ 0 V) to a pitting potential of + 0.5 V, held there for a certain duration, Δt, and then returned to the repassivation potential of 0 V. The latter allows the generated pits to be "frozen" in time, while subsequent x-ray diffuse scattering (XDS) scans were made. Fig. 4 shows the diffuse scattering profiles of the pitted copper surface at various holding times at + 0.50 V, e.g., 3, 4, 5, 7, and 9 minutes along with that taken at + 0.2 V where no pits were present on the surface. The peak centered at transverse momentum transfer $q_x = 0$ Å^{-1} is the specular reflection broadened by the experimental resolution and is well described by a Gaussian lineshape. The side lobes on both sides of the specular reflection are features associated with scattering from the pits. Similar side peaks have been observed in the diffuse scattering of Au or Pt surface deposition. [14]

Let us consider the expression (6) for the diffuse scattering. We may represent the statistical average of $|f(\bar{q}_1)|^2$ by $\exp(-4\pi^2 R^2 q_1^2)$, where R represents an average pit diameter. For $s(\bar{q}_1)$, the 2D structure factor of the pits (with the delta function at the origin, which arises from the average pit density subtracted because it contributes only to the specular reflectivity, as in Eq. (7)), we take the form suggested by Wu [15]

$$s(\bar{q}_1) = \frac{1}{1 + \frac{2\pi\phi_0}{q_1^2}\left[1 - \cos(q_1 d)\right]} \quad , \qquad (13)$$

where d is an average pit-separation and ϕ_0 the average surface density of the pits. Eq. (13) is based on a "hard-sphere" model for a 2D liquid. Eq. (6) with the above expressions was added to the specular reflectivity for a given q_z, and the result was then folded with the instrumental resolution function (assumed to be Gaussian, with a width obtained from the width of the specular in the absence of pitting), and was finally fitted to the observed transverse diffuse scans for that q_z. In these fits, R, d and ϕ_0 were taken as fitting parameters.

Because the incident illumination always has finite coherence across the interface, $S(\bar{q}_{\parallel})$ is to be understood as relating only to the pits within a single coherent region, and the overall intensity is to be summed over all such coherent regions across the interface. The consequence is that the factor $\phi A A_0$ in Eq. (6) is still proportional to the total number of pits on the interface N times $(A_0)^2$, whereas ϕ_0 in Eq. (13) refers to the average pit surface density within a single coherently scattering region and not the average over the whole interface. This is important in interpreting the results as discussed below.

The above method was used to fit the transverse scans, the parameters for

the background and the width of the Gaussian resolution function being obtained first by fitting to the scans obtained with an applied potential of + 0.2 V, where there were no pits. In Fig. 4, the fit to the experimental data for the 7 min. holding time at q_z of 0.15 $Å^{-1}$ is shown. The parameters of physical interest obtained from the fits are the number of pits N (to within a multiplicative constant), the average pit size R, the average pit separation d, and the average pit surface density ϕ_0. Eq. (6) was also used to fit the intensity of the maxima in the side lobes of XDS as a function of q_z with q_x held constant. For this purpose, the background was approximately subtracted by the same scan from an applied potential of + 0.2 V. Such a procedure can be used to obtain the depth distribution function $h(z)$.

In Fig. 5, the fit to the experimental data for the 7 min. holding time at q_z of 0.15 $Å^{-1}$ is shown. In Fig. 6, we show the parameters yielded from the fits for different holding times. The average nearest-neighbor distance of pits was found to decrease slightly from 8.5 μm to 7.5 μm for longer holding times, indicating a slight increase in the number density of the pits within each cluster. This is consistent with the fact that the position of the center of the side lobes shifted only slightly towards larger q_x for longer holding times. Furthermore, the maximum intensity of the side lobes was found to increase monotonically with Δt and by as much as five fold between the 3-min. and 9-min. mark, indicating the increase in the number of scattering objects. These two findings are consistent with the formation of clusters of pits. Within each individual cluster, there are many pits that have certain "short-range" order as manifested by the well-defined side lobes. At longer holding times, the number of clusters N_c increases, so does the number of pits per cluster N_p, but the nearest neighbor distance d remains nearly constant. Thus the average size of the cluster also increases. Finally, the average pit size was also determined, amounting to 4 μm at the 9-min. mark.

An important feature worth mentioning is the asymmetry of the XDS profiles. Rotation of the sample by 180° flipped the asymmetry of the scattering profile, confirming its genuine nature. The asymmetry is specially pronounced at the early stage of pit growth but less significant at later stages. This indicates that the shape of the pits in their initial state was inclined with respect to the surface normal (because of the preferred orientation of the crystal grains of the vacuum-evaporated Cu film) but became more symmetric as the pits grew bigger. This asymmetry suggests that pits are likely nucleated near crystalline defects such as grain boundaries or screw dislocations.

The depth distribution of the pits was determined from a measurement of intensity of the side lobes, I_{XDS}, as a function of q_z as shown in Fig. 7. The existence of a maximum in I_{XDS} indicates that the average pit depth has a bi-modal distribution, with the pits being preferentially distributed near the surface and at 40 Å from the surface. Also, the position of the maximum I_{XDS} was found to shift slightly towards a smaller value at longer holding times, indicating that the pits below the surface were becoming deeper during growth. With this physical interpretation, we modeled the measured data with two

Gaussian distributions separated by 40 Å, and the fit is shown by the solid line in Fig. 7. This bi modal distribution is consistent with the pitting mechanism of "film-breaking". [16] In this mechanism, pits are nucleated at the interface of the Cu oxide film and bulk Cu by transporting Cu through the oxide film and forming progressively bigger voids, leading eventually to film collapse. Therefore, there are two kinds of pits in coexistence in the early stages of pitting, one having the oxide film completely removed and thus exposed to the top surface and one being buried near the Cu oxide and Cu interface.

In summary, off-specular x-ray scattering provides a powerful *in-situ* probe of the morphology of thin films, such as polymer films that develop islands or holes, or of the morphology of localized corrosion pits on metal films in solution. For a copper electrode in 0-01M N_2HCO_3 solution, our results show that pitting proceeds in favor of pits clusters over individual pit growth. The number of pits in a cluster also increases with pitting time, as does the number of clusters. The diffuse scattering from these kinds of systems is the 2D analogue of small-angle scattering from hard sphere colloidal liquids, which has been so beautifully elucidated by S.H. Chen and his collaborators.

ACKNOWLEDGMENT

This work was supported by Corporate Research, Exxon Research & Engineering Co. and by the U.S. Department of Energy (U.S. DOE), office of Basic Energy Sciences, Division of Material Science under contract W-31-109-ENG-38. The NSLS facility is operated by the Brookhaven National Laboratory for the U.S. DOE. We thank G.J. Hughes, M. Pankuch, M. Sabella and the X10 beamline staff B. Zhang, S. Bennett, and M. Sansone for their help in carrying out the experiments at the NSLS.

REFERENCES

[1] S.K. Sinha, E.B. Sirota, S. Garoff, and H.B. Stanley, *Phys. Rev. B* 38 (1988) 2297; R. Pynn, *Phys. Rev. B* 45 (1992) 602.

[2] S.K. Sinha, S.K. Satija, T.P. Russell, E.B. Sirota, G.J. Hughes, A. Macrander, to be published.

[3] S.H. Anastasiadis, T.P. Russell, S.K. Satija, and C.F. Majkrzak, *Phys. Rev. Lett.* 62 (1989) 1852; and *J. Chem. Phys.* 92 (1990) 5677.

[4] T.P. Russell, A. Menelle, S.H. Anastasiadis, S.K. Satija, C.F. Majkrzak, *Macromolecules* 24 (1991) 6263.

[5] G. Coulin, D. Aussere, and T.P. Russell, *Phys. Rev. Lett.* 62 (1989) 1852.

[6] D.E. Savage, N. Schimke, Y.-J. Phang, and M.G. Lagally, J. Appl. Phys. 71 (1992) 3283; D.E. Savage, J. Kleiner, N. Schimke, Y.-H. Phang, T. Jankowski, J. Jacobs, R. Kariotis and M.G. Lagally, J. Appl. Phys. 69 (1991) 1411.

[7] S.K. Sinha, Physica B 173 (1993) 35; M.K. Sanyal, S.K. Sinha, A. Gibaud, S.K. Satija, C.F. Majkrzak and H. Homma, Mat. Res. Symp. Proc. 237 (1992) 393.

[8] Y. Liu, W. Zhao, X. Zhang, A. King, A. Singh, M.H. Rafailovich, J. Sokolov, K.H. Dai, E.J. Kramer, S.A. Schwarz, O. Gebizlioglu, and S.K. Sinha, *Macromolecules* 27 (1994) 4000.

[9] Z. H. Cai, K. Huang, P.A. Montano, T.P. Russell, J.M. Bai, and G.W. Zajac, J. Chem. Phys. 98 (1993) 2376.

[10] C. A. Melendres, Y. P. Feng, D. D. Lee, and S. K. Sinha, *J. Electrochem. Soc.* 142 (1995) L19.

[11] C. A. Melendres, H. You, V. A. Maroni, Z. Nagy, and W. Yun, *J. Electroanal. Chem.* 297 (1991) 549.

[12] H. You, C. A. Melendres, Z. Nagy, V. A. Maroni, W. Yun, and R. M. Yonco, *Phys. Rev. B* 45 (1992) 11288.
[13] J. G. N. Thomas and A. K. Tiller, *Br. Corros. J.* 7 (1972) 256.
[14] H. You, unpublished; I.K. Robinson, unpublished.
[15] Wen-li Wu, *J. Chem. Phys.*, 101 (1994) 4198.
[16] H. Böhni, *Langmuir* 3 (1987) 924.

Figure Captions

Fig. 1 Schematic of surface scattering experiment, using x-rays with incident angle wavevector $\bar{k}_0$, (grazing angle of incidence α), scattered wavevector $\bar{k}_1$, (grazing angle of scattering β). Longitudinal and transverse diffuse scans and the specular ridge are as indicated.

Fig. 2 Specular and longitudinal diffuse scattering as a function of q_z for a PS/PMMA (50:50), MW=30,000 film on a silicon substrate. The film is decorated with islands on the surface as discussed in the text. The fitted curves are not shown for clarity because they are almost indistinguishable from the experimental curves (from Ref. [2]).

Fig. 3 X-ray specular reflectivity of the copper electrode in $NaHCO_3$ solution at applied potentials (a) – 0.9 V, and (b) + 0.2 V.

Fig. 4 X-ray transverse off-specular reflectivity at the pitting potential of + 0.5 V after various holding times.

Fig. 5 Fit to the off-specular reflectivity after 7 minutes of holding time at the pitting potential of + 0.5 V.

Fig. 6 Time dependence of the average size, nearest-neighbor distance of pits within a cluster, the number of pits per cluster, and the number of clusters.

Fig. 7 X-ray longitudinal off-specular reflectivity at the pitting potential of + 0.5 V after various holding times.

Fig. 1

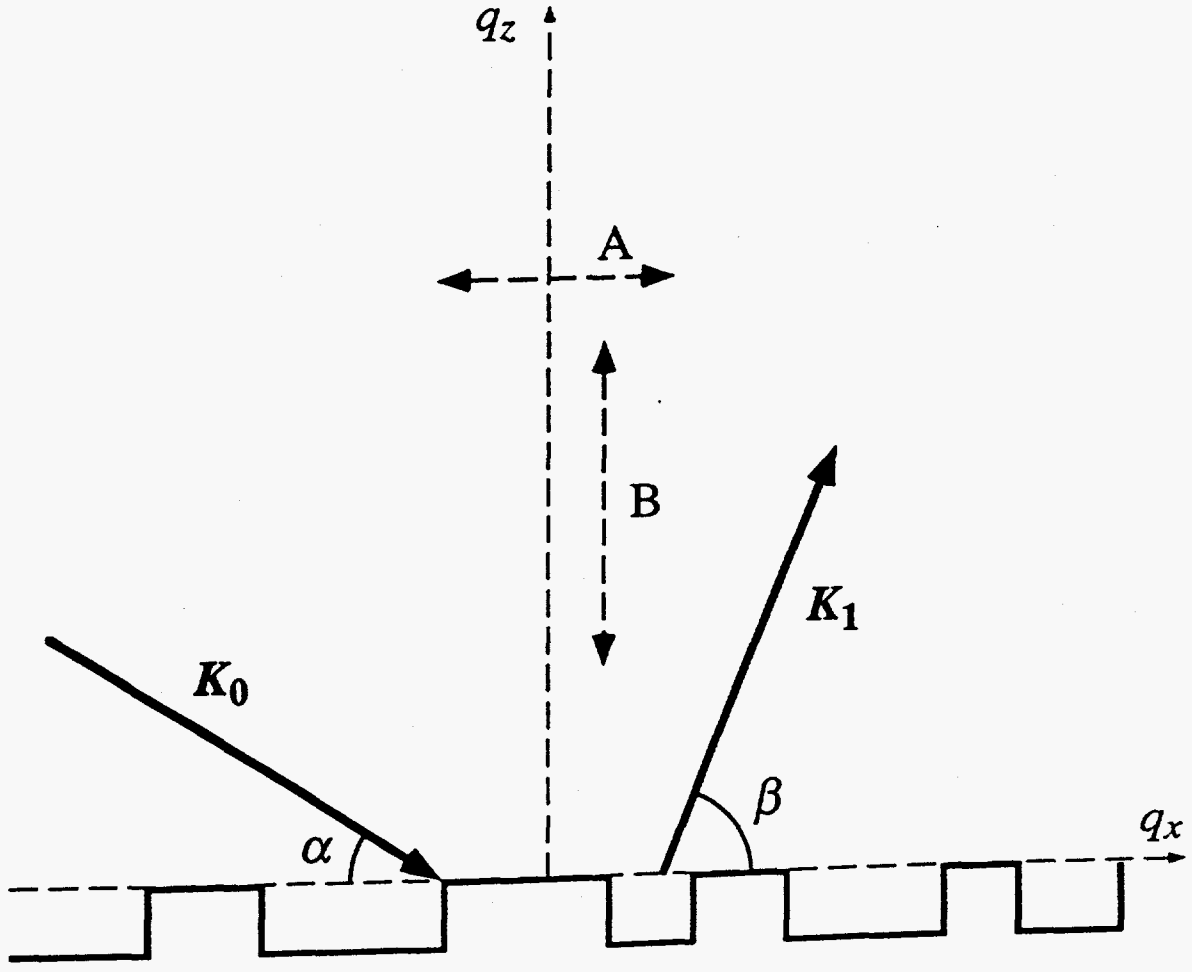

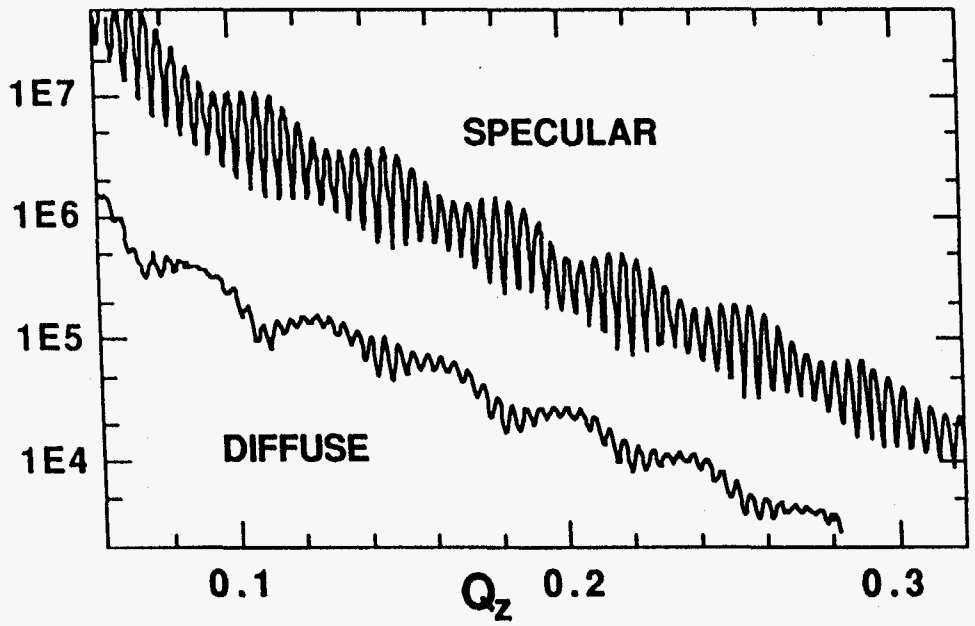
1E7
1E6
1E5
1E4
SPECULAR
DIFFUSE
0.1
0.2
0.3
Q_z

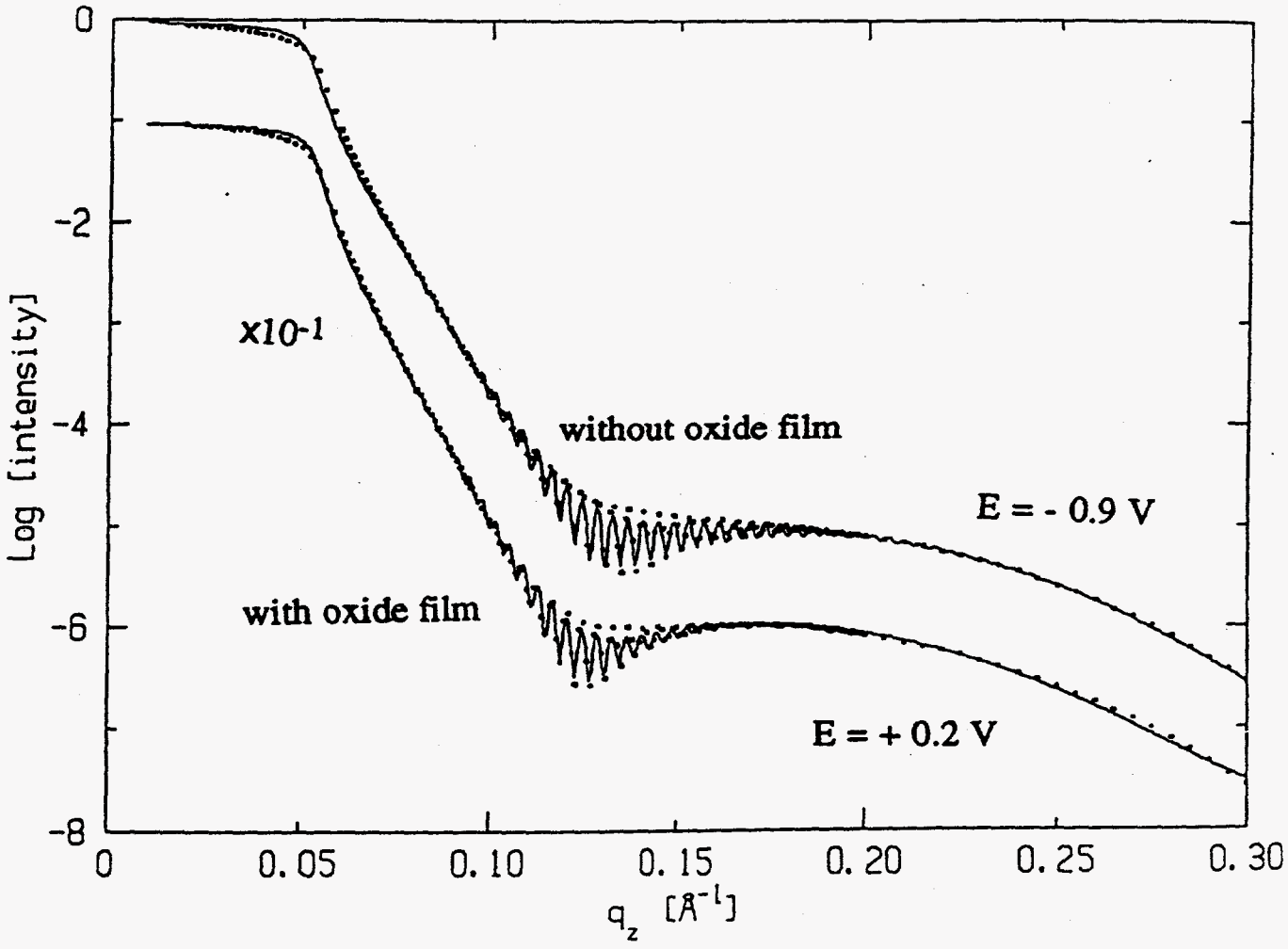
0
-2
-4
-6
-8
Log [intensity]
x10-1
without oxide film
E = - 0.9 V
with oxide film
E = + 0.2 V
0
0.05
0.10
0.15
0.20
0.25
0.30
qz [Å-1]

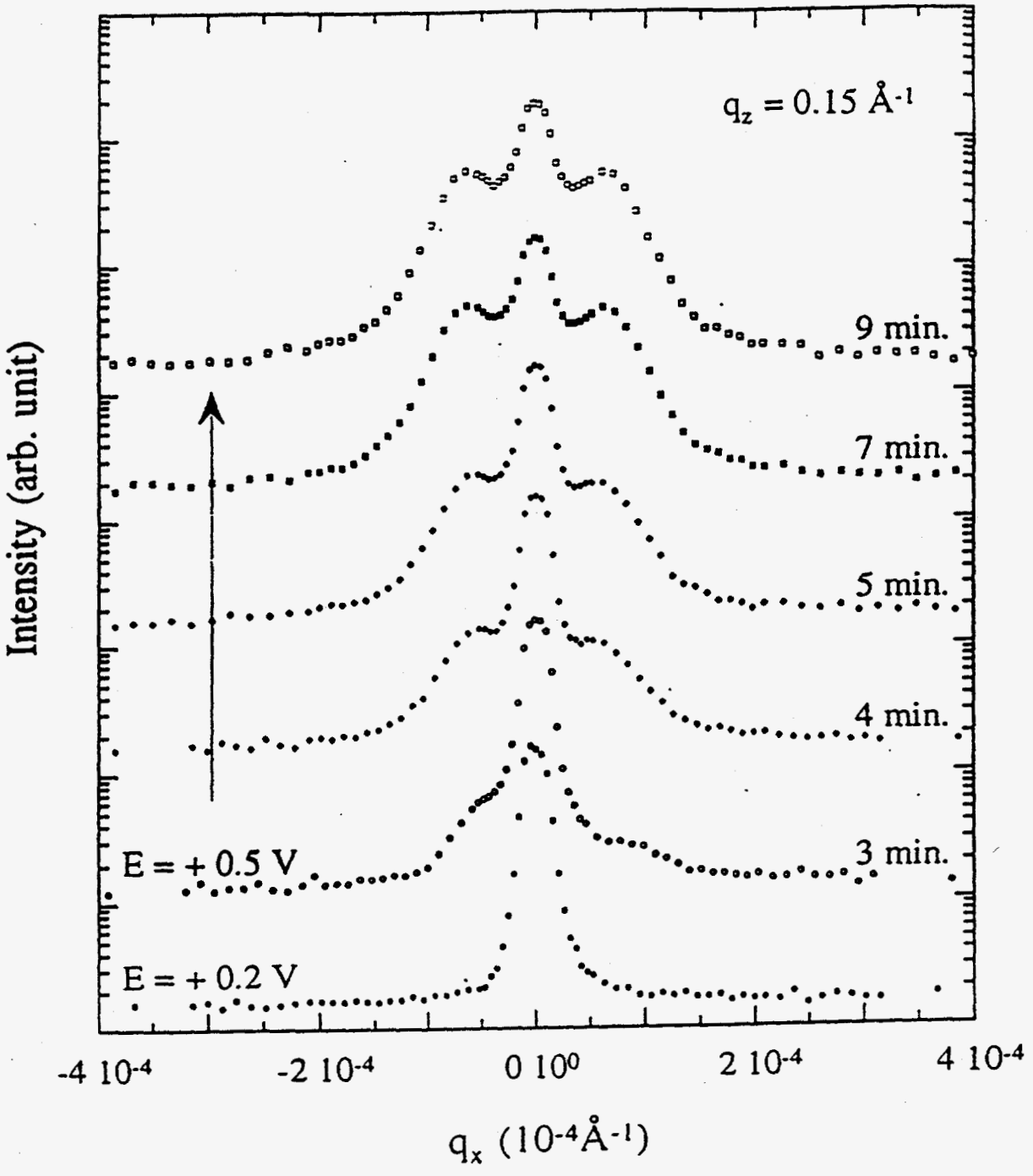
q_z = 0.15 Å^{-1}
9 min.
7 min.
5 min.
4 min.
3 min.
E = + 0.5 V
E = + 0.2 V
Intensity (arb. unit)
-4 10^{-4}
-2 10^{-4}
0 10^{0}
2 10^{-4}
4 10^{-4}
q_x (10^{-4}Å^{-1})

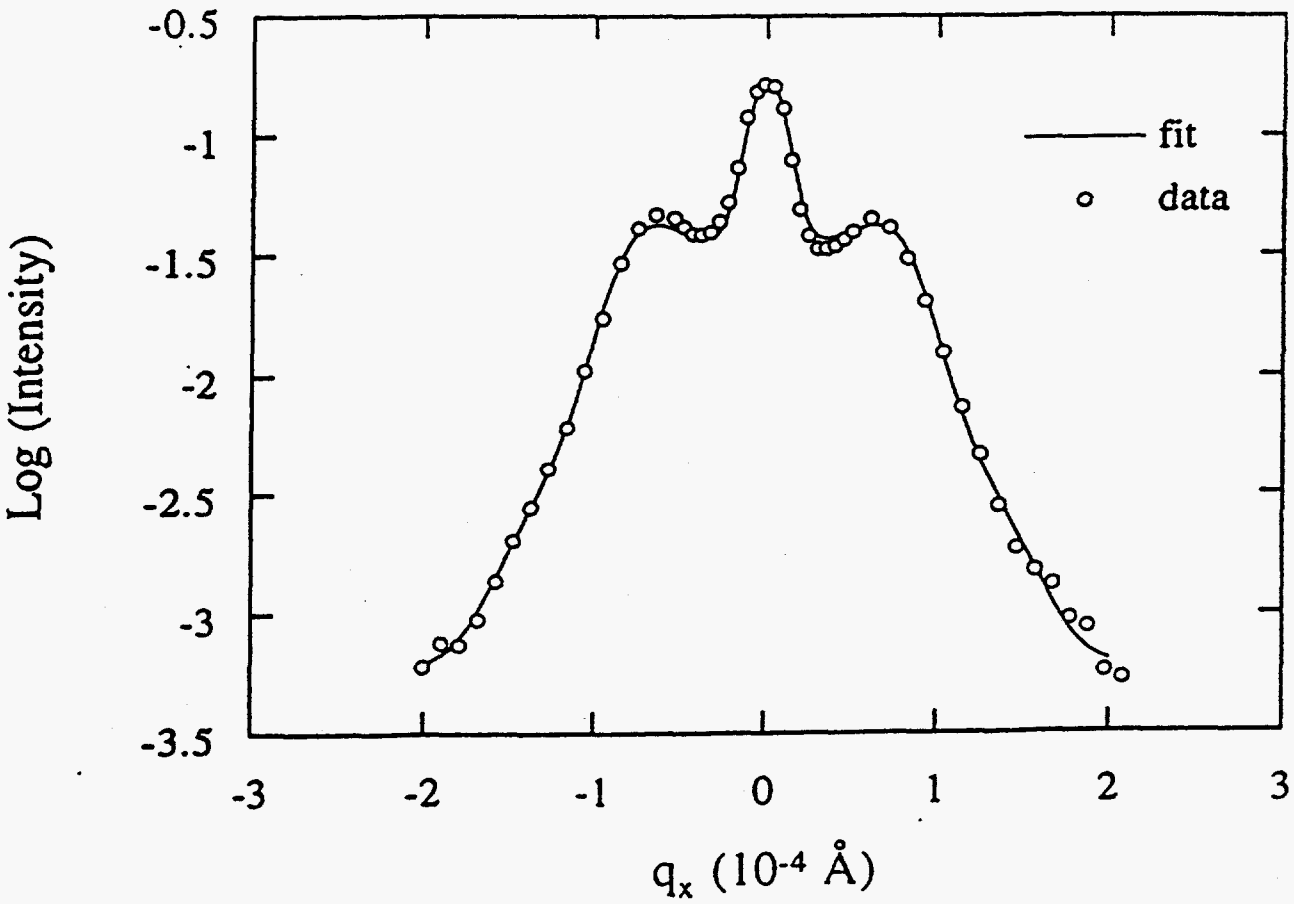
-0.5
-1
-1.5
-2
-2.5
-3
-3.5
Log (Intensity)
-3
-2
-1
0
1
2
3
q_x (10^{-4} Å)
fit
data

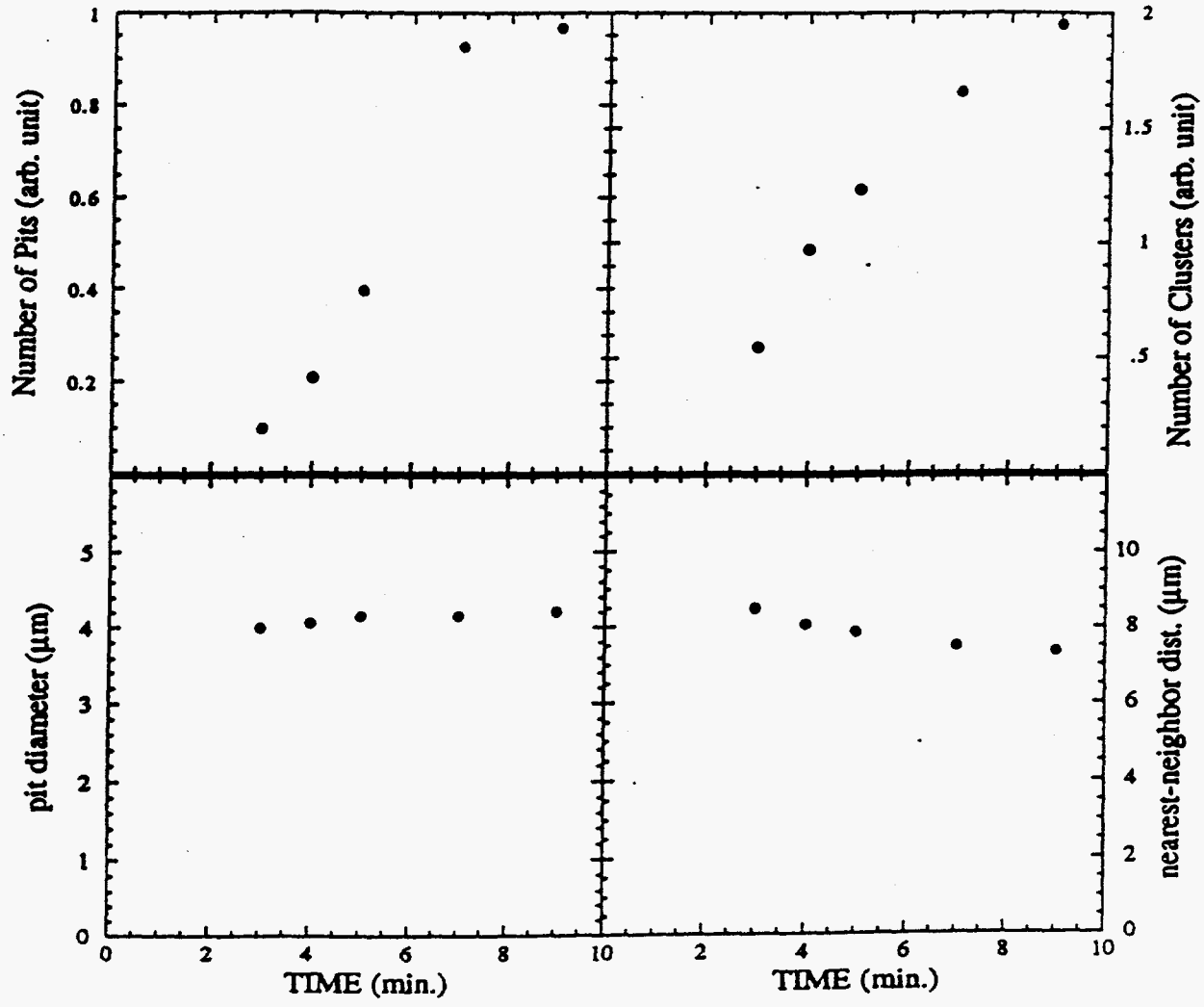
Number of Pits (arb. unit)
Number of Clusters (arb. unit)
pit diameter (μm)
nearest-neighbor dist. (μm)
TIME (min.)
TIME (min.)

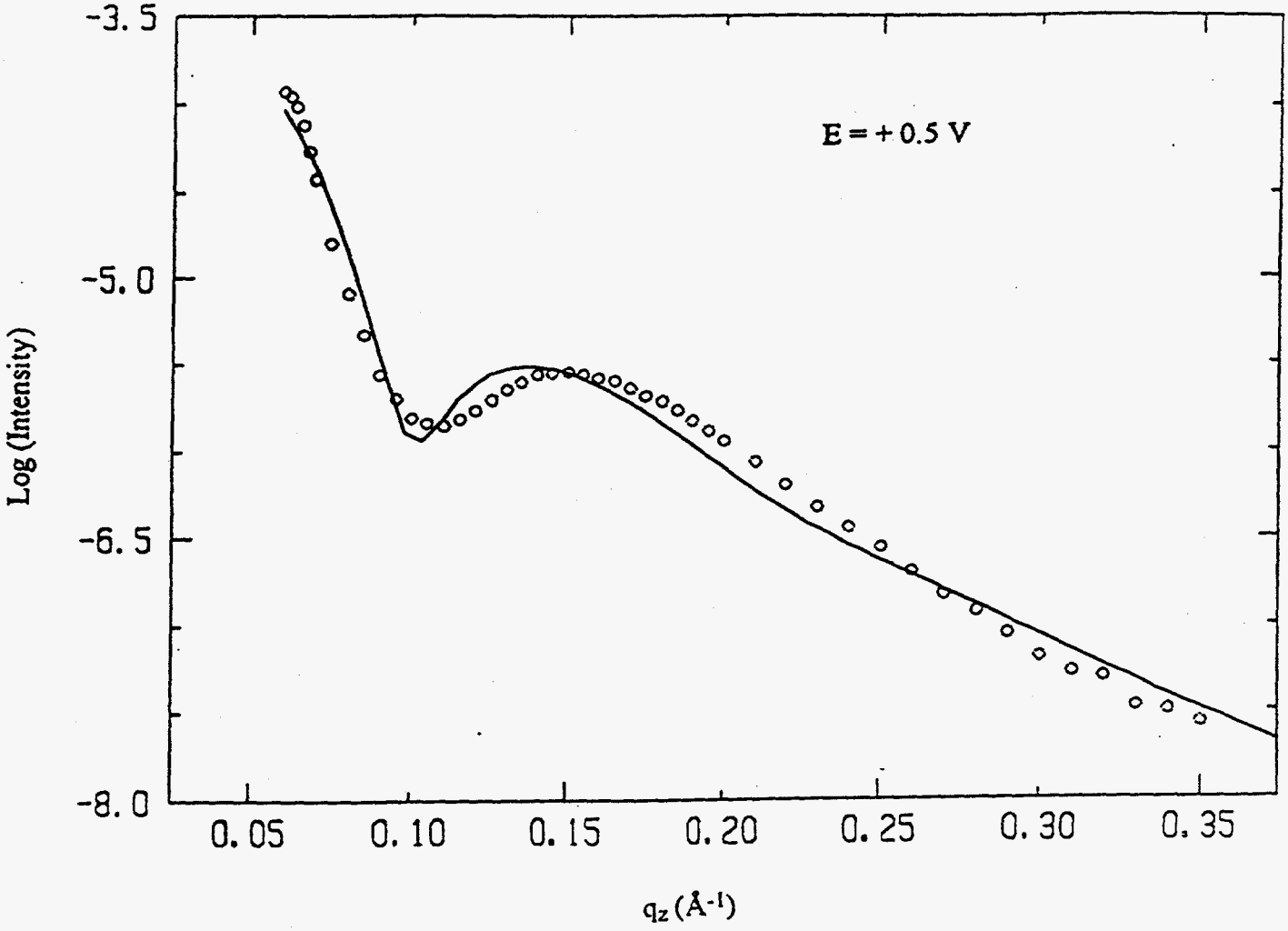

DISCLAIMER